Proposing a three-phase model for predicting the mechanical properties of mortar and concrete

Siventhirarajah Krishnya [1], Yogarajah Elakneswaran [1, *], Yuya Yoda [2]

[1] Division of Sustainable Resources Engineering

Faculty of Engineering, Hokkaido University

Kita 13, Nishi 8, Kita-ku, Sapporo, 060-8628, Japan

[2] Shimizu corporation

Shimizu Institute of Technology

Center for Construction Engineering, Japan

* Corresponding author

E-mail: elakneswaran@eng.hokudai.ac.jp (Y. Elakneswaran)

Tel: +81-11-706-7274

Abstract

The interfacial transition zone (ITZ) around aggregates is known as the weakest zone in mortar and concrete, which highly influences the mechanical properties. In this study, the influence of ITZ on mechanical properties such as Young's modulus and Poisson's ratio of cementitious materials is evaluated using a multi-scale model (developed in five hierarchical levels: nano-scale cement hydrates~ scale of concrete). In the proposed model, the microstructure of mortar/ concrete is considered as a three-phase material: fine/ coarse aggregates, ITZ of aggregates and bulk paste/ mortar. The primary input is the microstructure of cement paste and ITZ, which are predicted as the function of curing time using coupled cement hydration-thermodynamic model. The ITZ volume fraction is analytically computed based on aggregate particle size distribution. Multi-level homogenization methods (based on three-phase sphere model for two-phase composite material) are finally implemented to predict the effective properties of mortar and concrete. Here, the equivalent matrix consisted of fine/ coarse aggregate, bulk paste/ mortar and ITZ are obtained with the first and second levels homogenization procedures for mortar/ concrete. To validate the predictability of the models for mortar and concrete, predicted values are compared with independent experimental data sets. The results show a reasonable agreement with experimental results of Poisson's ratio and Youngs modulus (in the error range of 5 GPa). The influences of ITZ on properties of mortar and concrete are also discussed based on the outcomes.

Keywords: Mechanical properties; Mortar; Concrete; Multi-scale model; interfacial transition zone (ITZ); Homogenization approach

1. Introduction

Mortar and concrete are the most widely used building materials in the global construction industry. Owing to the diverse components such as cement hydrates, aggregates, and cement-aggregate interfacial zones, they highly reveal a complicated microstructure. Number of previous studies

disclosed that their behaviours on the application of loads are determined by intrinsic properties, which, at the micro-scale, are influenced by the water/cement ratio (w/c), clinker compositions and degree of hydration of cement, while aggregate properties play a significant role at the macroscale [1,2]. The properties of bulk paste existing in the matrix of mortar and concrete are time dependent. As the crystalline and semi-crystalline hydrates continue to evolve with hydration period, the materials become more complicated to understand [3,4]. Therefore, optical determination of the mechanical properties of mortar and concrete from their microstructure is of a great interest in industrial applications these days.

The occurrence of cement-aggregate interface (also referred to as interfacial transition zone, ITZ) is related to the wall-effect originated by the aggregate surface that disturbs the normal packing of cement particles [5–7]. During casting, the spatial arrangement of anhydrous grains becomes looser in the vicinity of aggregate particles. In addition, micro-bleeding of fresh mix leads to the accumulation of water near the surface of aggregate particles during the vibration of mixture and before setting. As the result, clinker content exhibits an increasing distribution with the distance from the aggregate surface, and a higher local w/c is attained in the ITZ of fresh mortar and concrete [5]. In fact, the ITZ is not a definite zone, but a region of transition, and a thickness ranging between 10–40 μm is documented for typical mortars and concrete [5,6,8,9]. Because of its high porosity compared to bulk paste matrix, ITZ is typically considered to reveal adverse effects on the performance of mortars and concretes, particularly on transport and mechanical properties to a great extent [5,6,8,9].

The thickness of the ITZ is found to be influenced by various casting factors such as curing age, w/c ratio, aggregates properties (type, roughness, shape and size), aggregate content and supplementary cementitious materials [6,10–13]. Recently, Huang et al. [13] investigated the ITZ properties of both normal aggregates and light weight aggregates. Their outcomes indicated that the ITZ between light

weight aggregate and cement paste is stronger and bonded without visible cracks compared to normal weight aggregates. High surface roughness of the lightweight aggregate can be the reason, which allows to have an effective mechanical interlocking, bringing advantages related to the strength of the aggregate-cement system. It should also be noted that w/c ratio at the interface would be low due to high water absorption of the lightweight aggregates, which leads to increased interfacial bonding strength in ITZ. Due to the tightened environmental policy on limiting aggregate exploitation and ever-increasing price, finding substitutes for natural aggregate has drawn a great deal of attention [14–16]. Involving artificial aggregates can be one potential alternative; following are some of such widely used materials: coal fly ash, paper ash, cement kiln dust, municipal solid waste incineration fly ash and bottom ash [17–19]. Jiang et al. [15] studied the performance of artificial aggregates on strength, ITZ and drying shrinkage, concluded that the artificial aggregates using waste concrete powder exhibits an enhancement on ITZ thickness, i.e., lower ITZ thickness (30 μm) was obtained for artificial aggregates compared to that of natural aggregate (60 μm) while improving mechanical properties of ITZ. This was attributed to the further reaction in aggregates located at the outer layer made by waste concrete powder with cement matrix, thus resulting in low porosity.

The concrete is characterized as a multi-phase material with several different representative scales. At macroscopic scale, concrete is regarded as a homogeneous material, while at mesoscopic scale, it is pondered to be consisting of coarse aggregates and mortar matrix [8]. Further subdivisions of the mortar matrix produce fine aggregates and hardened cement paste with pores embedded inside. It is well known that it is unsuitable to model the concrete at a single scale, as its intrinsic features range from nanometer-sized pores to millimeter-sized aggregates. Therefore, a multi-scale model can be more appropriate to link different length features of concrete, hence to evaluate macro-mechanical properties from micro-composition and micro-mechanical properties [20,21]. During the analysis, the properties computed at one scale, micrometers for instance, are inputted to the subsequent scale of the model, such as millimeters. For evaluating the effective properties of multi-inclusion composites

(such as mortar and concrete), homogenization stepping scheme was repeatedly shown to be an effective pathway [20–24]. In this homogenization method, the properties are assessed by averaging the stress and strain fields of material representative volume element (RVE) featuring a ‘‘mesoscopic” length scale which is much larger than the characteristic length scale of particles (inhomogeneities), but smaller than the characteristic length scale of a macroscopic specimen [20].

As yet, many research were undertaken to determine the Young’s modulus and Poisson’s ratio of concrete by both analytical and numerical methods. Earlier days, researchers attempted to model the concrete simply as a two-phase material consisting coarse aggregates and mortar matrix [25–27]. Although the two-phase model could provide approximate estimations, insightful results were not achieved. The variation between real values and estimated values (in two-phase models) was later found to be due to the ignorance of ITZ in concrete [25]. Thenceforth, the three-phase concept was incorporated by researchers in their models proposed to concrete by considering the ITZ as a single layer around aggregates [25,26]. It should be noted, however, modelling the ITZ realistically into the concrete composite was continuously a challenging process. For instance, during the prediction of Young’s modulus of concrete, Li et al. [28] failed to capture the overlapping between ITZs, which inevitably affected the accuracy of the prediction. In fact, the unavailability of experimental data on ITZ is the major hurdle that limits the developments of reliable and insightful simulations of concrete, which consequently leads the researchers to deal with lot of assumptions on properties of ITZ [20,29–31]. Particularly, in most of the existing models, the ITZ layer was assumed to be uniform with constant mechanical properties [5,30,32]. But, in real case, the clinker content in ITZ reveals a gradient increase with the distance from aggregate surface [6]. Moreover, by ignoring time-dependent effects, the mechanical properties of ITZ were assumed to be a specific ratio/ function of cement paste properties [29,31]. Therefore, it is still needed to develop reliable models by considering both gradient and time-dependent effects in ITZ for precise computations of Young’s modulus and Poisson’s ratio of concrete.

The model proposed in this research work systematically integrates (i) cement hydration model, (ii) thermodynamic model, (iii) multi-scale model and (iv) homogenization scheme to predict the mechanical properties of mortar and concrete in a realistic manner. By representing mortar/ concrete as a three-phase composite material and based on previously proposed model for w/c distribution in ITZ by Nedeau [6], the mechanical properties of ITZ and bulk paste/ mortar is computed with hydration period separately. Unlike most of the previously proposed models (wherein constant properties of ITZ and bulk paste were used), the computation of mechanical properties of ITZ and bulk paste is based on the detailed microstructure of hydrated cement paste including two types of C-S-H, capillary porosity, chemical shrinkage and other hydration products. Since the microstructure of cement matrix varies depending on curing time, chemical composition of clinker, w/c and curing temperature, the realistic computations of ITZ and bulk paste are emphasized in this proposed framework. Finally, the homogenization method is applied to predict the mechanical properties of the materials. The validity of the proposed model is verified with independent sets of experimental data, and the effect of ITZ on the Young's modulus and Poisson's ratio is investigated through sensitivity analysis for mortar and concrete.

2. Modelling strategy

The steps followed in the proposed model for mortar and concrete are clearly depicted in **Figure. 1**. The fundamental parameters such as clinker compositions, properties of clinker and aggregates, mixture recipe and boundary conditions are the necessary input parameters for computations. As conceptually illustrated in **Figure. 2**, both the mortar and concrete are considered as three-phase materials: (i) mortar: fine aggregates, ITZ and bulk paste, and (ii) concrete: coarse aggregates, ITZ and mortar. It should be noted, as the ITZ consists of low amount of clinker and high amount of water, it can be reasonably considered as a cement paste with higher w/c (compared to the initial w/c of fresh concrete mix/ mortar mix). The required mechanical properties of ITZ and bulk paste are separately

157 computed from the cement paste model developed in our previous work [33]. Finally, homogenization
158 method was used to predict the mechanical properties of mortar and concrete. The elaboration of
159 modelling approach can be found in subsequent sections.

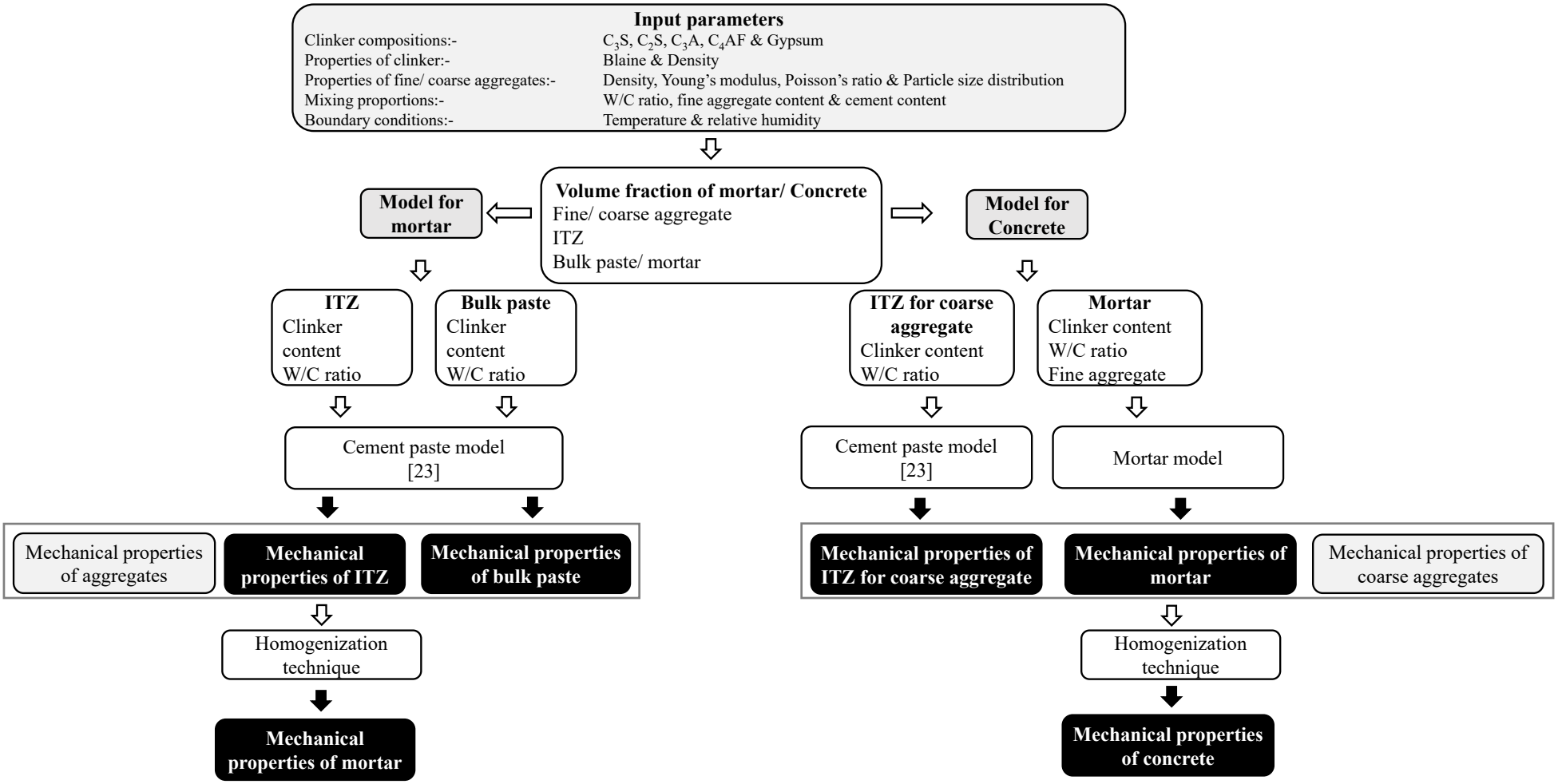

Figure. 1. Flow diagram of the model proposed for mortar and concrete

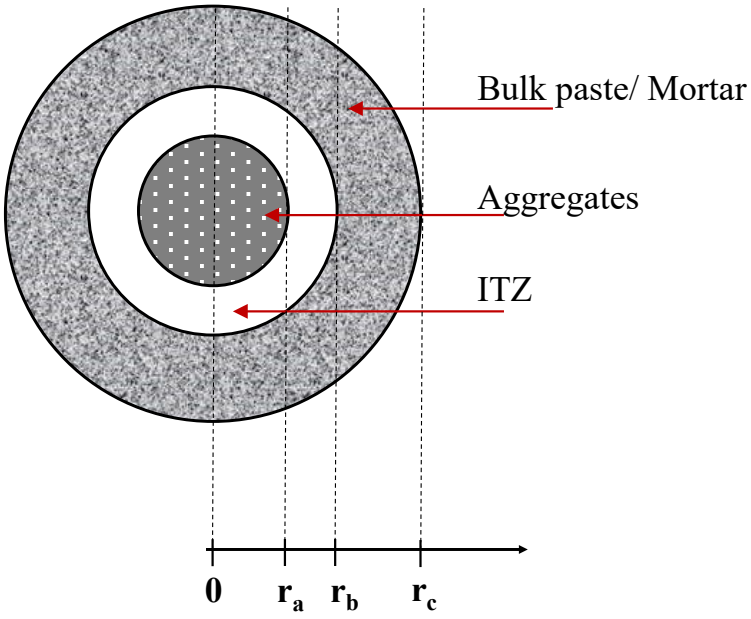

163

164

165 **2.1 Properties of ITZ**

166 The development of ITZ imposes adverse effect on the mechanical properties; therefore, the
167 properties of ITZ such as volume fraction and mechanical properties are required to be predicted in a
168 realistic manner. As discussed earlier, the aggregate properties are one of the parameters that
169 determine the thickness of the ITZ [34,35], and the mechanical properties of ITZ vary with the
170 hydration period. Therefore, for a specific degree of hydration (i.e., for a specific curing period), the
171 ITZ can be considered as a single shell with uniform mechanical properties. Moreover, based on the
172 previous studies, the thickness is presumed to be 15 μm for fine aggregate in mortar and 40 μm for
173 coarse aggregate in concrete [36–38].

174

175 The volume fraction of aggregate in typical concrete is more than 60%, thereby the spacing between
176 adjacent aggregates can only be a few times the typical ITZ thickness [39,40]. Similar to that
177 implemented in previous studies, the volume fraction of ITZ is computed herein by considering the
178 overlapping of ITZ shells using the 'void exclusion probability' [41]. Principally, the void exclusion
179 probability is the volume fraction of the space not occupied by all the spheres and ITZ shells, i.e.,

fraction of the bulk paste. Hence, the ITZ volume fraction f_{ITZ} for an ITZ thickness of h can be expressed as,

$$f_{ITZ} = (1 - f_{agg})(1 - \exp(-\pi\rho(\alpha_1 h + \alpha_2 h^2 + \alpha_3 h^3))) \quad (1)$$

where,

$$\alpha_1 = \frac{4\langle R^2\rangle}{1-f_{agg}} \quad (2)$$

$$\alpha_2 = \frac{4\langle R\rangle}{1-f_{agg}} + \frac{12\in_2\langle R^2\rangle}{(1-f_{agg})^2} \quad (3)$$

$$\alpha_3 = \frac{4}{3(1-f_{agg})} + \frac{8\in_2\langle R\rangle}{(1-f_{agg})^2} + \frac{16A\epsilon_2^2\langle R^2\rangle}{3(1-f_{agg})^3} \quad (4)$$

$$\in_2 = \frac{2\pi\langle R^2\rangle}{3} \quad (5)$$

with A being equal to 2, 3, and 0 for the Carnahan-Starling, scaled- particle, and Percus-Yevick approximation, respectively [41]. However, by comparing with numerical exact model data, Garboczi and Bentz [42] suggested that $A = 0$ is always the best choice for the simulation, thus, A is taken as zero in this work. ρ is the total number of aggregates per unit volume, and α_1, α_2 and α_3 are functions of mean aggregate radius $\langle R\rangle$ and mean square aggregate radius $\langle R^2\rangle$ according to the aggregate size distribution. According to previous studies [42,43], with the assumption of uniform distribution by volume of aggregates, the remaining parameters are calculated from aggregate size distribution as,

$$\rho = \sum \frac{9 f_{agg} f_i}{4\pi(r_{i+1}^3 - r_i^3)} ln\frac{r_{i+1}}{r_i} \quad (6)$$

$$\langle R^n\rangle = \sum \frac{9 f_{agg} f_i}{4\pi\rho(r_{i+1}^3 - r_i^3)} \int_{r_i}^{r_{i+1}} r^{n-1}\, dr \quad (7)$$

f_{agg} is the volume fraction of aggregate. f_i is the fraction of the total volume of aggregate that has a radius between r_i and r_{i+1}, $r_i < r_{i+1}$. A typical sieve analysis is expressed in terms of the mass fraction passing or retained by a certain sieve size, which can easily be converted to the form given

here. If aggregates of different size have all the same density, then mass fractions are the same as volume fractions. Once the ITZ volume fraction is known, the volume fraction of bulk paste (f_{bulk}) is obtained by simple subtraction.

To represent the concrete or mortar of practical use, the proportion of each phase constituent in the composite sphere should satisfy the following conditions (refer to **Figure. 2**) [35].

$$f_{agg} = \frac{r_a^3}{r_c^3} \tag{8}$$

$$f_{agg} + f_{itz} = \frac{r_b^3}{r_c^3} \tag{9}$$

The local volume fraction of anhydrous cement in bulk paste ($\alpha_{c,bulk}$) and ITZ ($\alpha_{c,ITZ}$) are computed from Nadeau [6]. Moreover, the effective w/c of bulk paste and ITZ is calculated based on Eq 10.

$$w/c_{bulk\ or\ ITZ} = \frac{1-\alpha_{c,bulk}\ or\ \alpha_{c,ITZ}}{\rho_c \alpha_{c,bulk}\ or\ \alpha_{c,ITZ}} \tag{10}$$

2.2 Multi-scale model

In computational material science, concrete is characterized as a multi-phase material with different representative scales [8]. At mesoscopic scale, it is focused to be consisting of coarse aggregates and mortar matrix; the mortar matrix can be subdivided as fine aggregates and hardened cement paste; the hardened cement paste consists of several hydration products, unreacted clinker and capillary porosity. Therefore, a multi-scale model can be more appropriate for realistically predicting the behaviour of concrete and evaluating the impact of compositions on the mechanical properties. **Figure. 3** presents the organization of the multi-scale model proposed in this study, describing the levels and constitutions for modelling the concrete.

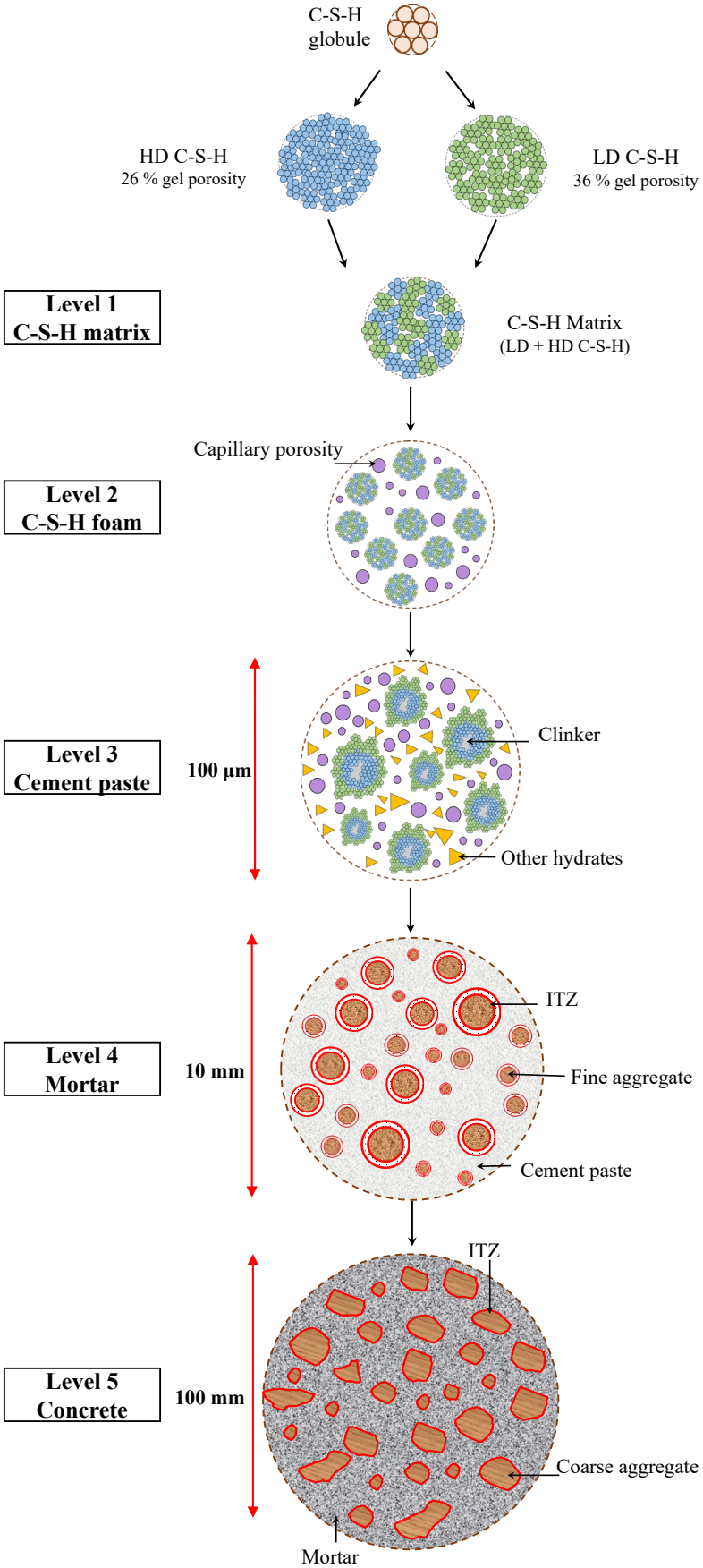

Figure. 3. Representation of hierarchical model (multi-scale) proposed for concrete

2.2.1 Model description for cement paste

The development of cement paste model (Level 1-3 of the multi-scale model) is described briefly in this section. It should be noted that further detail of cement paste model can be found in our previous work [33]. Here, as the first step, the popular hydration model proposed by Parrot and Killoh [44] was implemented to predict the hydration products based on the considered input parameters such as clinker composition, boundary condition and mixing conditions. Thermodynamic calculations were performed using the open source geochemical (IPHREEQC) based on the estimated dissolution rate of clinker minerals to predict the hydration products. Using the predicted volume fraction of hydration products such as two types of C-S-H (Low density C-S-H and High density C-S-H), portlandite, ettringite, monosulfate, hydrotalcite, Fe-siliceous hydrogarnet and calculated chemical shrinkage based on the reaction rate of each clinker minerals, the capillary porosity with hydration period was predicted. The multi-scale model initiating from C-S-H matrix (Level 1) and ending up with cement paste (Level 3) was then used to predict the mechanical properties of cement paste. **Figure. 4** depicts the overall procedure adopted in the cement paste model.

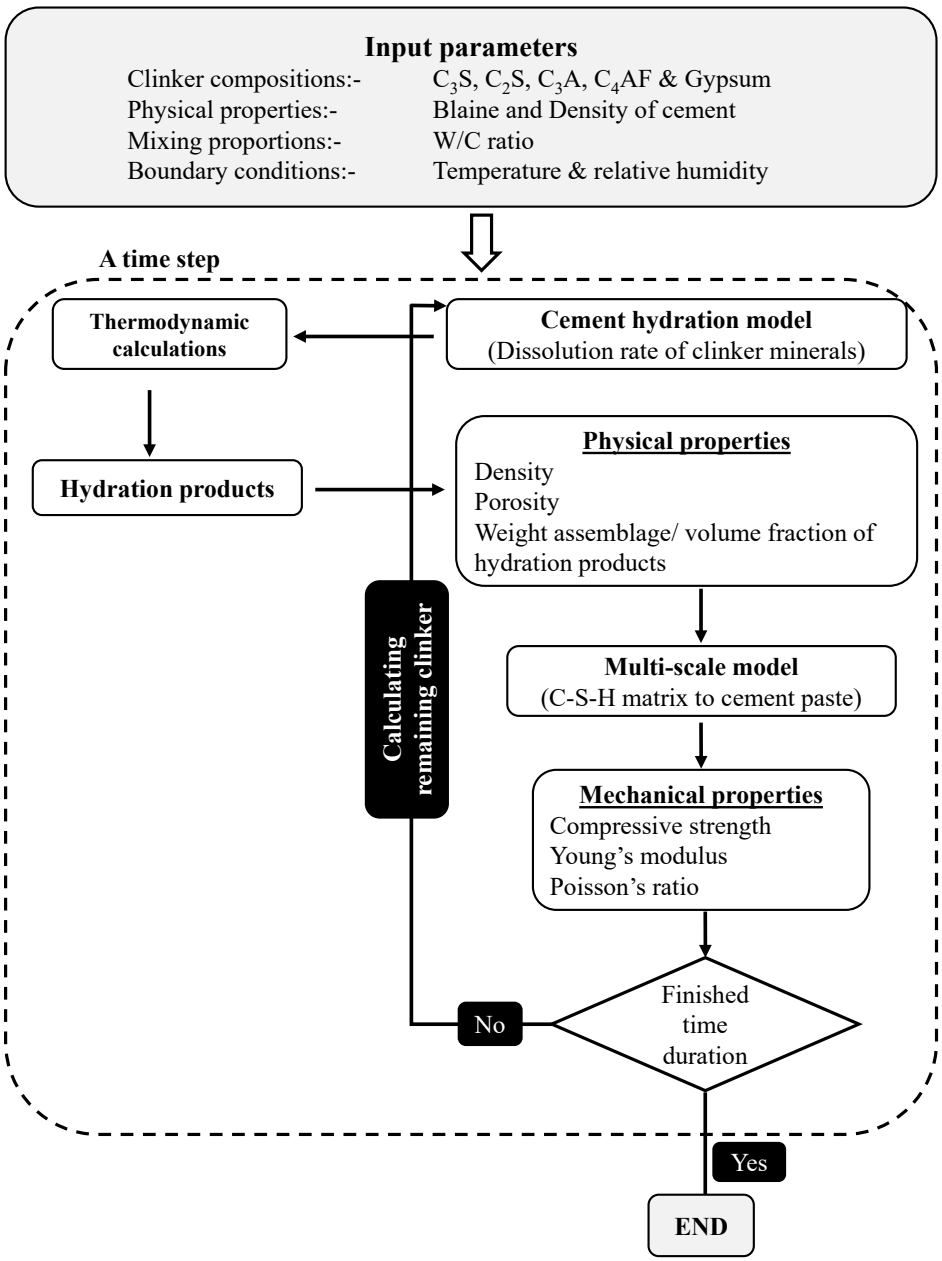

246 **Figure. 4.** Flow diagram illustrating the procedure used to develop the cement paste model
247

248 **2.2.2 Model description for mortar**

249 In the model proposed for mortar, the aggregate is assumed to be inert with the cement in order to
250 eliminate the complexity of the model. The properties of ITZ and bulk paste vary with w/c ratio,
251 degree of reaction, aggregate content, and clinker properties. As illustrated in **Figure. 1**, to predict
252 the mechanical properties of ITZ and bulk paste, following parameters are required: (i) clinker content,
253 (ii) w/c ratio and (iii) volume fraction of ITZ and bulk paste. Clinker content in ITZ and bulk paste is
254 obtained from Nadeau [6], while the w/c ratio and volume fraction are computed using Eq. 10 and
255 Eq. 1, respectively. The above-mentioned computations are then inputted to cement paste model

(which is the integration of cement hydration model, thermodynamic model, and multi-scale model) to predict the mechanical properties. The predicted mechanical properties (of ITZ and bulk paste), volume fraction of all three phases and considered mechanical properties of fine aggregate are finally used to predict the mechanical properties of mortar such as Young's modulus and Poisson's ratio using the homogenization method (as illustrated in **Figure. 5**).

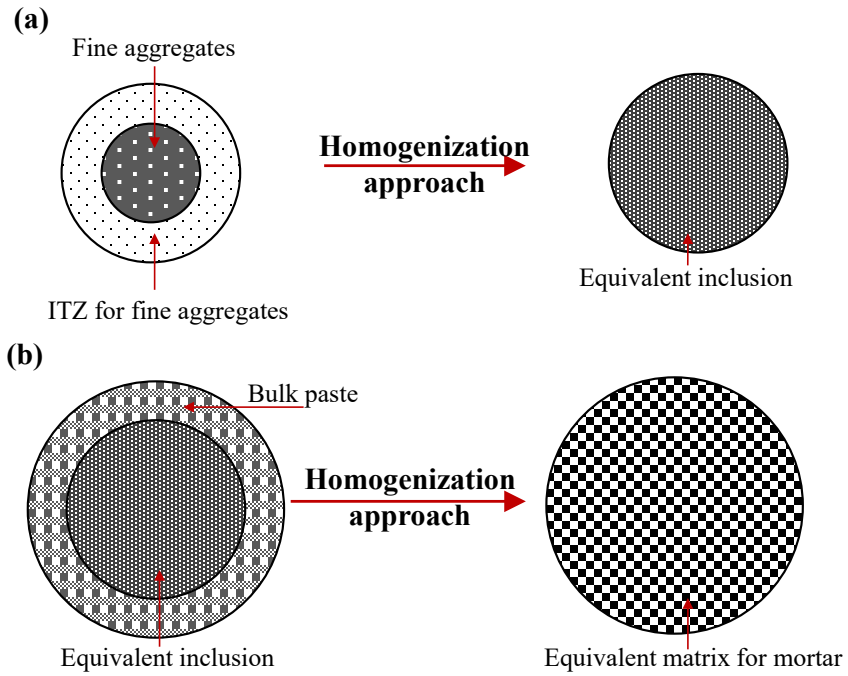

Figure. 5. Two step homogenization procedure of mortar: **(a)** the first step homogenization of fine aggregates and ITZ and **(b)** the second step homogenization of equivalent inclusion and bulk paste

The two-step homogenization method employed herein was developed by Christensen and Lo [45]. The method is based on three-phase sphere model for two-phase composite material, which was developed to compute the effective bulk and shear modulus by assuming that each individual aggregate has homogeneous particle size with equivalent elastic properties and radius. The origin of this model was from the study by Eshelby [45]. Following the evaluations, Christensen [45] concluded that the homogenization model can be more reliable than other generally used models such as differential scheme and Mori-Tanaka model [46], because the stress-strain field interactions between different inclusions were considered in this model [47]. This homogenization model was

also implemented in several previous studies to predict the effective properties of mortar and concrete [20,47]. As per the first step, the effective properties of two-phase composite made up of fine aggregates and ITZ (shown in **Figure. 5(a)**) are computed based on Eq. 11- Eq. 19 [45].

$$K_{equ} = K_{ITZ} + \frac{\emptyset_{agg}(K_{agg}-K_{ITZ})(3K_{ITZ}+4G_{ITZ})}{3K_{ITZ}+4G_{ITZ}+3(1-\emptyset_{agg})(K_{agg}-K_{ITZ})} \quad (11)$$

$$B\left(\frac{G_{equ}}{G_{ITZ}}\right)^2 + C\left(\frac{G_{equ}}{G_{ITZ}}\right) + D = 0 \quad (12)$$

$$B = 8\left(\frac{G_{agg}}{G_{ITZ}} - 1\right)(4 - 5\nu_{ITZ})\eta_1\emptyset_{agg}^{\frac{10}{3}} - 2\left(63\left(\frac{G_{agg}}{G_{ITZ}} - 1\right)\eta_2 + 2\eta_1\eta_3\right)\emptyset_{agg}^{\frac{7}{3}} +$$

$$252\left(\frac{G_{agg}}{G_{ITZ}} - 1\right)\eta_2\emptyset_{agg}^{\frac{5}{3}} - 50\left(\frac{G_{agg}}{G_{ITZ}} - 1\right)(7 - 12\nu_{ITZ} + 8\nu_{ITZ}^2)\eta_2\emptyset_{agg} + 4(7 - 10\nu_{ITZ})\eta_2\eta_3 \quad (13)$$

$$C = -4\left(\frac{G_{agg}}{G_{ITZ}} - 1\right)(1 - 5\nu_{ITZ})\eta_1\emptyset_{agg}^{\frac{10}{3}} + 4\left(63\left(\frac{G_{agg}}{G_{ITZ}} - 1\right)\eta_2 + 2\eta_1\eta_3\right)\emptyset_{agg}^{\frac{7}{3}} -$$

$$504\left(\frac{G_{agg}}{G_{ITZ}} - 1\right)\eta_2\emptyset_{agg}^{\frac{5}{3}} + 150\left(\frac{G_{agg}}{G_{ITZ}} - 1\right)(3 - \nu_{ITZ})\nu_{ITZ}\eta_2\emptyset_{agg} + 3(15\nu_{ITZ} - 7)\eta_2\eta_3 \quad (14)$$

$$D = 4\left(\frac{G_{agg}}{G_{ITZ}} - 1\right)(5\nu_{ITZ} - 7)\eta_1\emptyset_{agg}^{\frac{10}{3}} - 2\left(63\left(\frac{G_{agg}}{G_{ITZ}} - 1\right)\eta_2 + 2\eta_1\eta_3\right)\emptyset_{agg}^{\frac{7}{3}} +$$

$$252\left(\frac{G_{agg}}{G_{ITZ}} - 1\right)\eta_2\emptyset_{agg}^{\frac{5}{3}} + 25\left(\frac{G_{agg}}{G_{ITZ}} - 1\right)(\nu_{ITZ}^2 - 7)\eta_2\emptyset_{agg} - 3(5\nu_{ITZ} + 7)\eta_2\eta_3 \quad (15)$$

$$\eta_1 = \left(\frac{G_{agg}}{G_{ITZ}} - 1\right)(49 - 50\nu_{agg}\nu_{ITZ}) + 35\left(\frac{G_{agg}}{G_{ITZ}}\right)(\nu_{agg} - 2\nu_{ITZ}) + 35(2\nu_{agg} - \nu_{ITZ}) \quad (16)$$

$$\eta_2 = 5\nu_{agg}\left(\frac{G_{agg}}{G_{ITZ}} - 8\right) + 7\left(\frac{G_{agg}}{G_{ITZ}} + 4\right) \quad (17)$$

$$\eta_3 = \frac{G_{agg}}{G_{ITZ}}(8 - 10\nu_{ITZ}) + (7 - 5\nu_{ITZ}) \quad (18)$$

$$\emptyset_{agg} = \frac{f_{agg}}{f_{agg}+f_{ITZ}} \quad (19)$$

where K_{equ} and G_{equ} are the effective bulk modulus and shear modulus of the equivalent inclusions after the first step of homogenization. K_{agg}, G_{agg} and ν_{agg} are the bulk modulus, shear modulus and Poisson's ratio of fine aggregates. K_{ITZ}, G_{ITZ} and ν_{ITZ} are the bulk modulus, shear modulus and Poisson's ratio of ITZ, and which are obtained from the previous work [33].

Since the mortar consisting of bulk paste and equivalent inclusion (as elucidated in **Figure. 5(b)**), the effective mechanical properties of mortar can be similarly computed by homogenization approach. The Eq. 11 - Eq. 19 are amended by replacing the effective properties of equivalent inclusion ($\emptyset_f$, G_{equ}, K_{equ} and ν_{equ}) and bulk paste properties (G_{bulk}, K_{bulk} and ν_{bulk}) in the place of aggregate properties ($\emptyset_{agg}$, G_{agg}, K_{agg} and ν_{agg}) and ITZ properties (G_{ITZ}, K_{ITZ} and ν_{ITZ}) to predict effective bulk modulus and shear modulus of mortar (K_{mor}, G_{mor}). The formula for volume fraction of equivalent inclusion in mortar is provided in Eq. 20. The bulk paste properties (G_{bulk}, K_{bulk} and ν_{bulk}) are obtained from the previous work [33].

$$\emptyset_f = \frac{f_{agg} + f_{ITZ}}{f_{agg}+ f_{ITZ}+ f_{bulk}} \quad (20)$$

$$E_{mor} = \frac{9K_{mor}G_{mor}}{3K_{mor}+G_{mor}} \quad (21)$$

$$\nu_{mor} = \frac{3K_{mor}-2G_{mor}}{2(3K_{mor}+ G_{mor})} \quad (22)$$

Theoretically, two sets of moduli are required for the computation of Young's modulus and Poisson's ratio of a material; therefore, bulk modulus of mortar (K_{mor}) together with shear modulus of mortar (G_{mor}) were used herein to predict the Young's modulus (E_{mor}) and Poisson's ratio (ν_{mor}) from the

316 fundamental relationship presented in Eq.21 and Eq. 22. Finally, the predicted results were validated
317 using experimental results.
318
319 **2.2.3 Model description for concrete**
320 In the proposed model (refer **Figure. 1**), concrete is reliably assumed as three phase material
321 consisting of coarse aggregate, ITZ and mortar. In order to eliminate the complexity of the simulation,
322 coarse aggregate is considered as chemically inactive with cement paste similar to that considered for
323 fine aggregate. The volume fraction of ITZ for coarse aggregate ($f_{C.ITZ}$) is computed with aid of Eq.
324 1 using the particle size distribution of coarse aggregate and ITZ thickness. Similar procedure that
325 has been described for mortar is used to estimate the clinker content and w/c in ITZ for coarse
326 aggregate and mortar (existing in concrete). Based on the computed w/c and clinker content, the
327 mechanical properties of ITZ paste is predicted using the cement paste model [33]. Besides, the
328 mechanical properties of mortar are predicted using the computed w/c, clinker content and fine
329 aggregate content as described in section 2.2.1. The predicted mechanical properties (of ITZ and
330 mortar), volume fraction of all three phases and considered mechanical properties of coarse aggregate
331 are finally used to predict the mechanical properties of concrete using the homogenization method
332 (illustrated in **Figure. 6**).

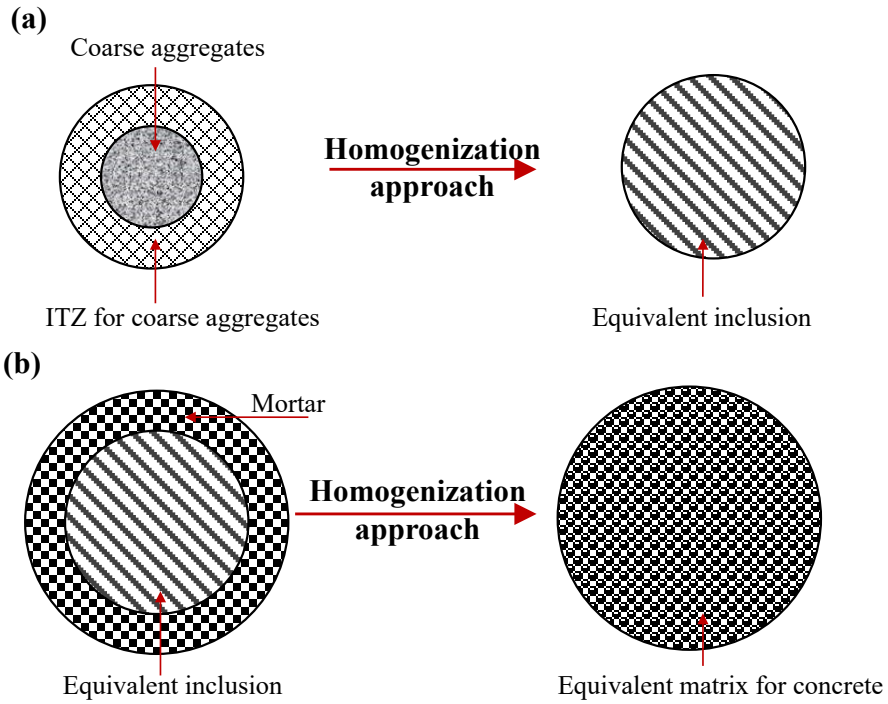

Figure. 6. Two step homogenization procedure for concrete: **(a)** the first step homogenization of coarse aggregates and ITZ and **(b)** the second step homogenization of equivalent inclusion and mortar matrix

As elucidated in **Figure. 6(a)**, the coarse aggregates and ITZ are considered in the first step. The Eq. 11 – Eq. 19 has been modified by replacing coarse aggregates properties ($\emptyset_{C.agg}$, $G_{C.agg}$, $K_{C.agg}$ and $\nu_{C.agg}$) and ITZ properties of coarse aggregates ($G_{C.ITZ}$, $K_{C.ITZ}$ and $\nu_{C.ITZ}$) in the place of fine aggregates properties ($\emptyset_{agg}$, G_{agg}, K_{agg} and ν_{agg}) and ITZ properties of fine aggregates (G_{ITZ}, K_{ITZ} and ν_{ITZ}) to predict the bulk ($K_{equ,\ con}$) and shear modulus ($G_{equ,\ con}$) of equivalent inclusion for concrete. The formula for volume fraction of coarse aggregate in equivalent inclusion is given in Eq. 23.

$$\emptyset_{C.agg} = \frac{f_{C.agg}}{f_{C.agg}+f_{C.ITZ}} \tag{23}$$

where, $f_{C.agg}$ is the volume fraction of coarse aggregate in concrete.

In the second step, the equivalent inclusion and mortar matrix are considered for the homogenization method as shown in **Figure. 6(b)**. The effective mechanical properties of concrete can be similarly computed by homogenization approach. The Eq. 11 - Eq. 19 were altered by replacing the effective properties of equivalent inclusion ($\emptyset_{C.f}$, $G_{equ,con}$, $K_{equ,con}$ and $\nu_{equ,\ con}$) and mortar properties (G_{mor}, K_{mor} and ν_{mor}) in the place of coarse aggregate properties ($\emptyset_{C.agg}$, $G_{C.agg}$, $K_{C.agg}$ and $\nu_{C.agg}$) and ITZ properties of coarse aggregates ($G_{C.ITZ}$, $K_{C.ITZ}$ and $\nu_{C.ITZ}$) to predict effective bulk modulus and shear modulus of concrete (K_{Con}, G_{Con}). The volume fraction of equivalent inclusion in concrete is given in Eq. 24.

$$\emptyset_{C.f} = \frac{f_{C.agg} + f_{C.ITZ}}{f_{C.agg} + f_{C.ITZ} + f_{mor}} \tag{24}$$

where, f_{mor} is volume fraction of mortar in concrete. Once the volume fraction of ITZ for coarse aggregate is known, the volume fraction of mortar (f_{mor}) is obtained by simple subtraction ($f_{mor} = 1 - f_{C.agg} - f_{C.ITZ}$).

The Young's modulus (E_{Con}) and the Poisson's ratio (ν_{Con}) of concrete are predicted from the fundamental relationship presented in Eq. 21 and Eq. 22 by replacing the concrete moduli in the place of mortar properties. Finally, the predictability of the model is validated using the experimental results available in the literature.

3. Results and discussion

3.1 Sensitivity analysis of ITZ

Figure. 7 presents the Young's modulus of mortar and concrete predicted as a function of hydration period for different ITZ thickness. It should be mentioned that the prediction corresponds to the w/c of 0.6. The considered volume fraction of fine aggregate for mortar is 0.6, and cement: fine aggregate:

coarse aggregate weight ratio for concrete is 1: 1.5: 3.2. The results clearly demonstrate that increasing the thickness of the ITZ results in a reduction in predicted Young's modulus. It is well known that the ITZ is the weakest zone in mortar and concrete [48]. The increase in ITZ thickness directly upsurges the volume fraction of ITZ, leading to the decrease in effective elastic modulus of the mortar and concrete. Similar behavior was observed by Simeonov and Ahmad [26] and Li et al. [28]. However, when the ITZ thickness exceeds 15 μm for mortar and 40 μm for concrete, the predicted results do not show significant variation (refer **Figure. 7**). It is apparent that the volume fraction of ITZ increases with the increasing thickness, yet the volume fraction of bulk paste decreases, ensuing a negative effect on effective Young's modulus. Meanwhile, the local w/c in ITZ and bulk paste increases with ITZ thickness based on the model proposed by Nadeau [6], which leads to a positive effect on modulus. Since the above effects compromise each other, further increase in ITZ thickness does not show significant reduction in final outcomes. Relatively a similar ITZ thickness (in a range between 10-50 μm) was also reported for sand and coarse aggregates in many previous works [5,6,8,9]. On the above basis, therefore, the ITZ thicknesses of 15 and 40 μm are reliably chosen for the computations in the proposed model.

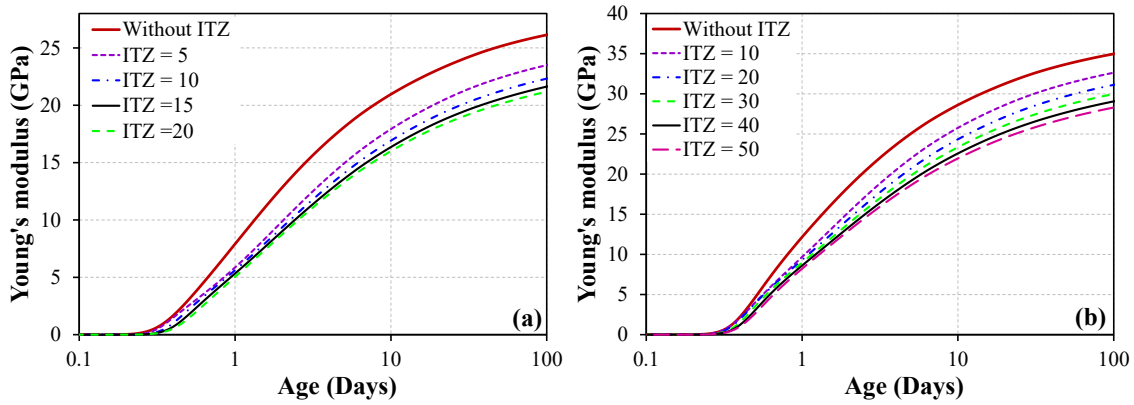

3.2 Young's modulus of mortar

To reveal the predictability of the proposed model, the predicted Young's moduli of mortar are compared with two independent sets of experimental results (refer **Figure. 8** and **Figure. 9**). In **Figure. 8**, the raw experimental data were employed for the comparison. The experimental conditions and procedures corresponding to the set of data compared in **Figure. 8** are detailed in **Appendix A.** The data used in **Figure. 9** for validating the predicted results were obtained from previous report [49]. The comparisons indicate that the predicted results exhibit a good agreement with the both experimental sets for range of w/c and aggregate volume fractions. Slight variations are however witnessed in certain readings. For instance, 5 GPa variation could be seen between experimental and predicted results for the mortar with w/c of 0.4, aggregate volume fraction of 0.6 and curing period of 28 days (in **Figure 8**). It should be noted that in computations, the Young's modulus and Poisson's ratio of fine aggregate were considered to be 37.7 GPa and 0.2 respectively [50].

Regardless of w/c and aggregate volume fractions, the Young's modulus increases with hydration period. Besides, relatively higher values are predicted for the mortar with lower w/c, which is in consistent with that of hydrated cement paste. This could mainly be attributed to the increased formation of prime binding agent (i.e., C–S–H) at low w/c during the hydration. In due course, the decrease in the porosity could lead to the development of denser microstructure [33], resulting an increase in Young's modulus of mortar matrix with hydration period. Moreover, for a specific w/c ratio, high moduli are computed for high content of fine aggregate (refer to **Figure. 8** and **Figure. 9**). This is because of the increased stiff inclusion in the paste and decreased effective water content, which lead to the decrease in porosity in bulk paste [10,51]. The tendencies predicted herein for Young's modulus of different cases are in consistent with those reported in previous studies [29,49,52–54].

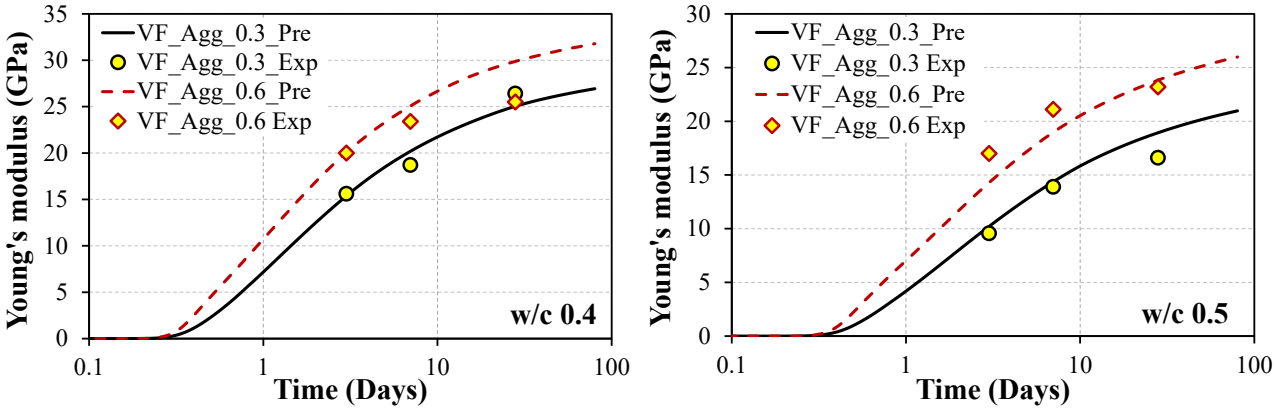

420

421

422 (VF_Agg stands for volume fraction of aggregate)

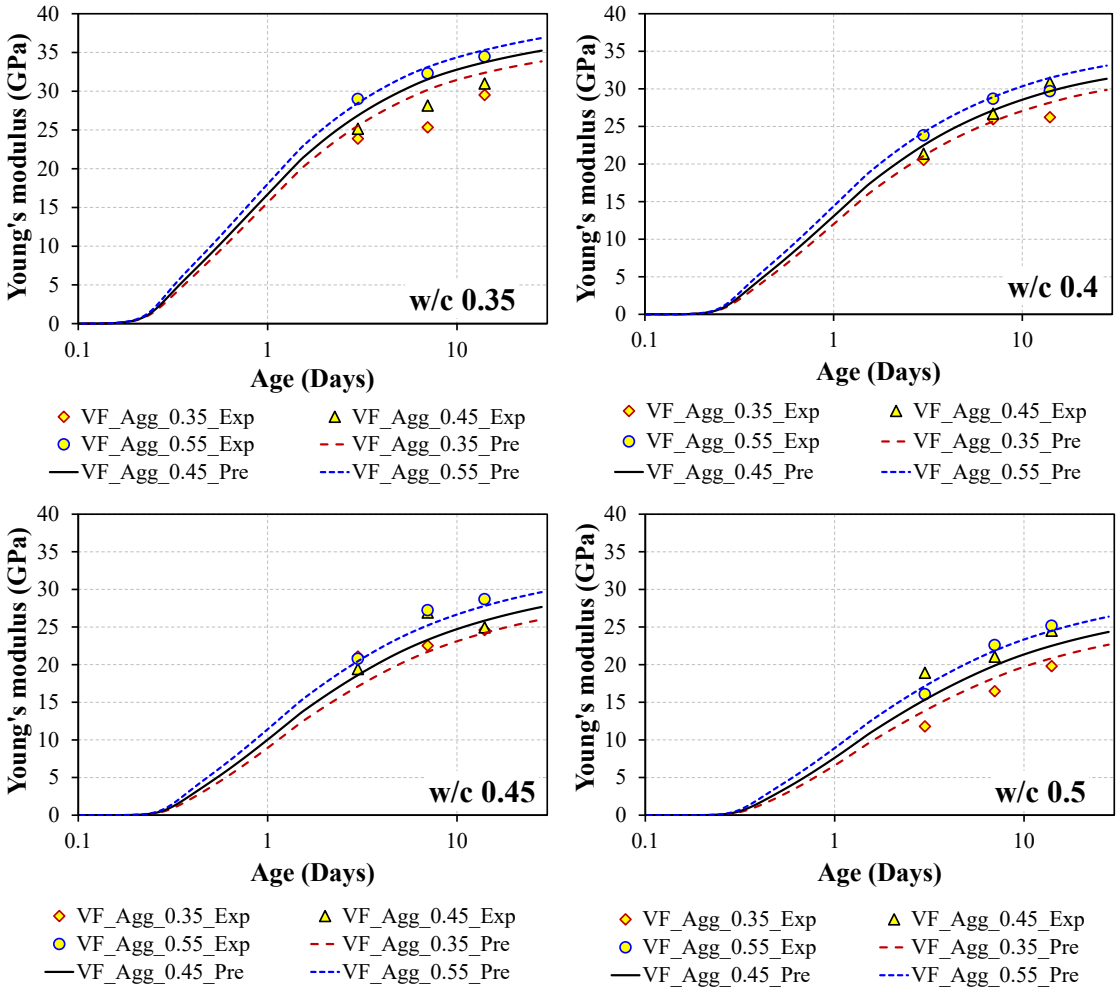

423

424

425 aggregate 0.35-0.55 (the experiment results were obtained from ref. [49]) (VF_Agg stands for

426 volume fraction of aggregate)

427

Figure. 10 presents the compilation of predicted Young's modulus plotted against the experimental results of mortars corresponding to w/c ratios ranging from 0.3 to 0.55 and aggregate volume fraction from 0.2 to 0.6. The experimental data were obtained from both measurements and literature [49,53]. As illustrated in **Figure. 10**, the predicted results of Young's modulus fall within the error range of 5 GPa for all three sets of experiment results. Based on the sets of comparisons (**Figure. 8**, **Figure. 9,** and **Figure. 10**), it is perceived that the proposed model can be reliable for predicting the Young's modulus of mortar with different w/c ratios and aggregate volume fractions.

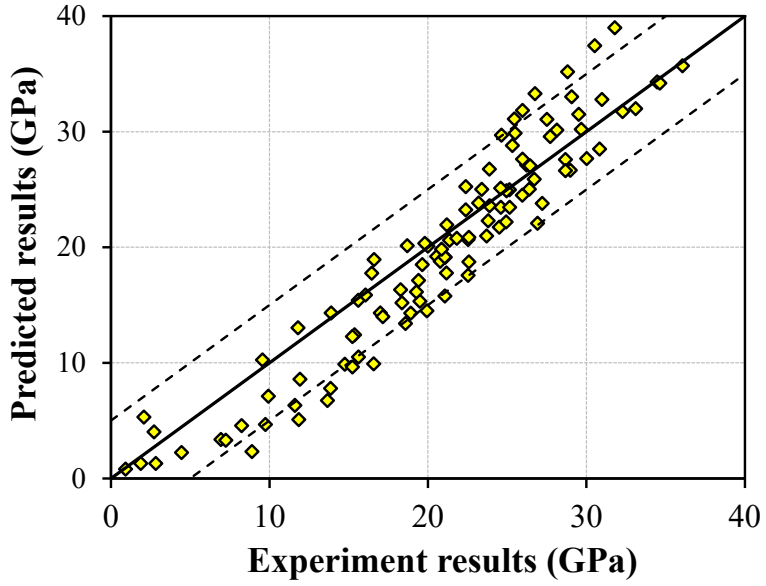

3.3 Poisson's ratio of mortar

Figure. 11 presents the variation of Poisson's ratio of mortar with hydration period for w/c of 0.3, 0.4 and 0.5 and fine aggregates volume fraction of 0.3 and 0.6 (The experimental conditions and procedures corresponding to the experiment data presented in **Figure. 11** are detailed in **Appendix A.**). It can be observed that the predicted results appear to slightly overestimate the Poisson's ratio for w/c ratio of 0.5, while those show a better agreement with experimental results for the w/c ratios of 0.3 and 0.4. The tendency observed for w/c ratio of 0.5 increases with increasing hydration period,

which is in contrast with those observed for other w/c ratios. In fact, during the early stage, the mortar exists in suspension form within the water, thus the Poisson's ratio of fresh mix is equal to Poisson's ratio of water (0.5) [55,56], and which is captured by the proposed model (**Figure. 11**). When the hydration is in progress, the Poisson's ratio of mortar decreases due to the formation of denser microstructure by replacing the solids in the place of water. Thus, the increasing tendency observed for w/c of 0.5 might be due to experimental error. It can also be noticed that the Poisson's ratio increases with the increase in w/c ratio, which is similar to the tendency observed for cement paste [33,57]. For a specific water cement ratio, the Poisson's ratio decreases with the increase in volume fraction of fine aggregates (refer to **Figure. 11**). It is clear that sand is considerably stiffer than the cement paste; therefore, the increasing stiffer inclusions in paste tends to restrain the lateral expansion of the softer matrix. In fact, both Young's modulus and Poisson's ratio of the aggregate influence the elastic properties such as Poisson's ratio and elastic modulus of mortar [58].

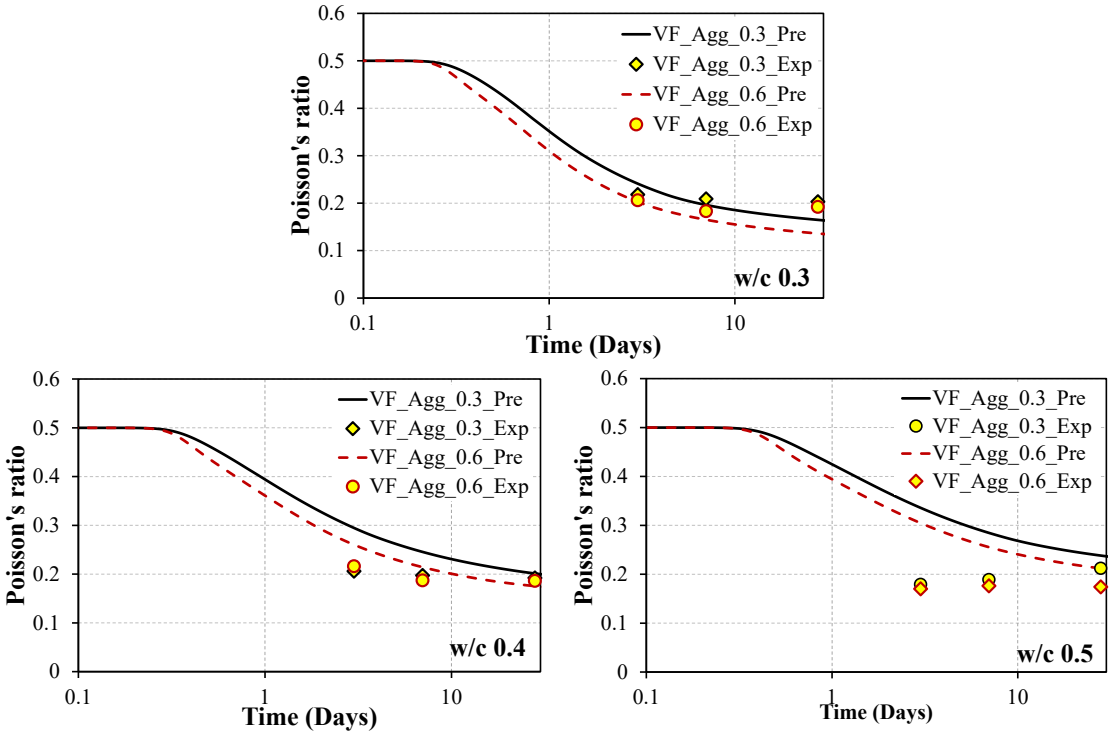

Figure. 11. Validation of Poisson's ratio of the mortar for w/c 0.3-0.5 with volume fraction of aggregate 0.3 and 0.6 (VF_Agg stands for volume fraction of aggregate)

3.4 Young's modulus of concrete

Figure. 12 and **Figure. 13** illustrate the predictability of the model for the Young's modulus of concrete with two independent sets of experimental results obtained from previous studies. **Figure. 12** shows the comparison of Young's modulus for different w/c ratio and different types of cement (Type I and Type V). The experiment results used herein for the comparison belong to Han and Kim [59]. The second set of experimental data compared in **Figure. 13** were obtained from Corinaldesi and Moriconi [60] for w/c, volume fraction of fine aggregate and volume fraction of coarse aggregates of 0.56, 0.12 and 0.5, respectively. During the computation, the Young's modulus and Poisson's ratio of coarse aggregates were considered to be 50 GPa and 0.18, respectively [61], and for the fine aggregates, they were respectively 37.7 GPa and 0.20. Based on the considered aggregates properties, the proposed model shows a good capability to predict the Young's modulus of concrete for different w/c and wide range of aggregates content. There are however slight variations observed for some points (refer **Figure. 12**), which could possibly be due to the assumptions made during prediction. Since the required parameters such as particle size distribution and properties of aggregates (Young's modulus and Poisson's ratio) were not available in the literature, they were assumed based on the instructions given in literature. Additionally, the aggregates were assumed to be inert and ITZ properties to be constant with distance from aggregate for a specific time. Nevertheless, the development of Young's modulus of concrete reveals almost a similar tendency of the development of Young's modulus of mortar.

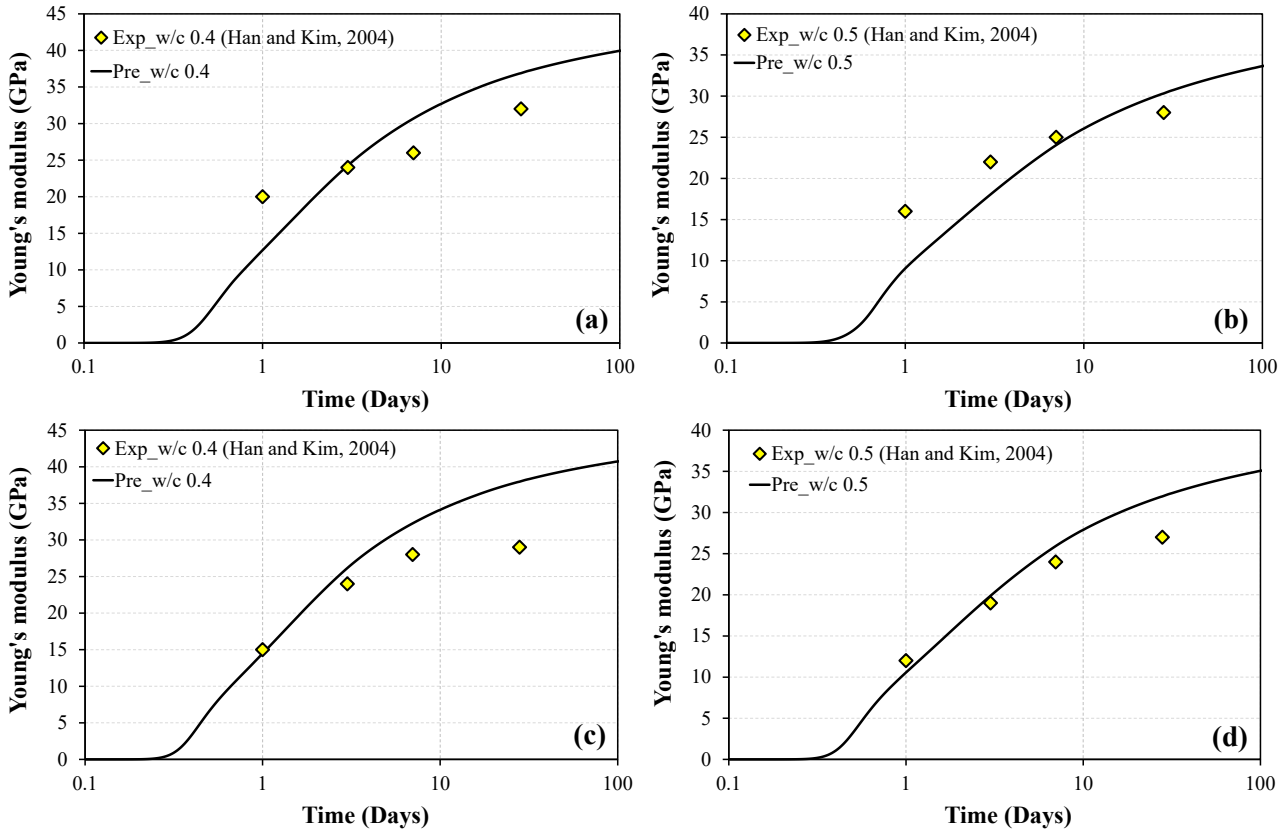

Figure. 12. Validation of Young's modulus of concrete (experiment results were obtained from ref. [59] of **(a)** and **(b)** for Type I cement and **(c)** and **(d)** for Type V cement.

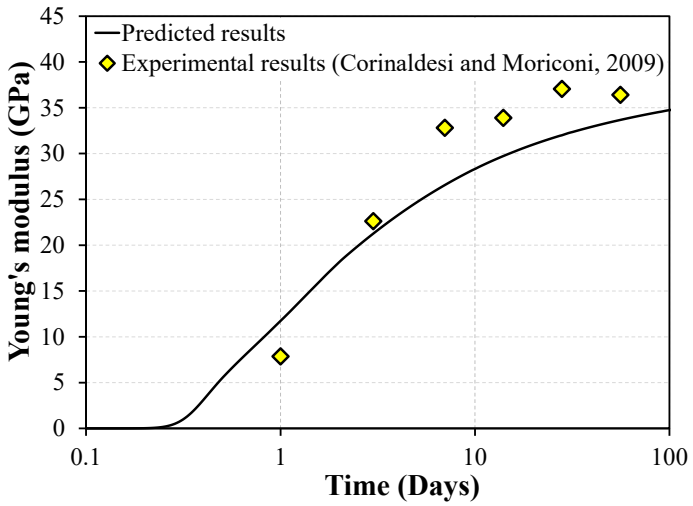

Figure. 13. Validation of Young's modulus of concrete (experiment results were obtained from ref. [60])

Figure. 14 shows the overall validation for 30 number of measured Young's modulus of concrete with the w/c of 0.4 to 0.6. All the experiment results were taken from previous studies [59,60,62]. The predicted results of Young's modulus fall within the error range of 5 GPa for all three sets of experiment results as depicted in **Figure. 14**. Based on the sets of validations (**Figure. 12**, **Figure. 13** and **Figure. 14**), it is verified that the proposed model can be reliable for predicting the Young's modulus of concrete with different w/c ratios and aggregate volume fractions.

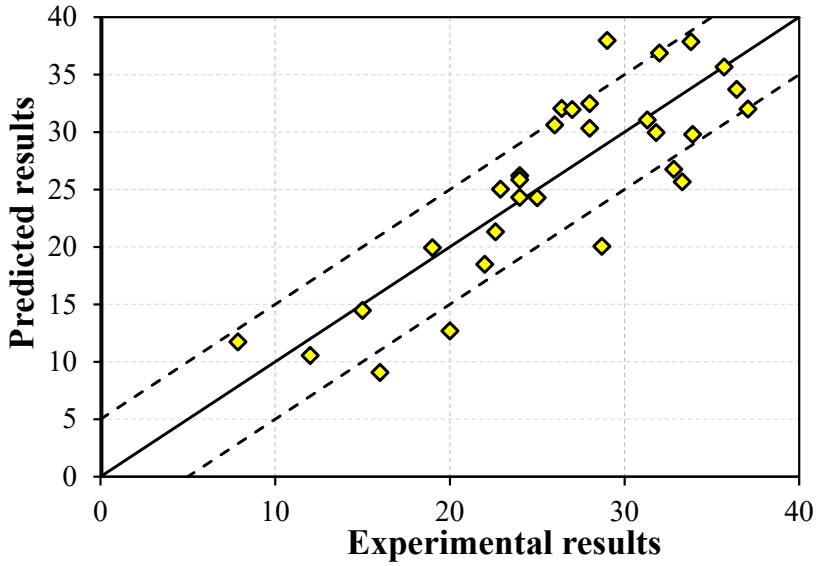

Figure. 14. Comparison of predicted Young's modulus plotted against the experiment results

3.5 Poisson's ratio of concrete

The validation of Poisson's ratio with hydration period of concrete for w/c of 0.5, sand to cement ratio of 1.5 and coarse aggregate to cement ratio of 3 is presented in **Figure. 15**. The experiment results used for the comparison were taken from Allos and Martin [63]. The predicted results show relatively good agreement with experiment results (after 10 days); however, the model appears to overpredicts the Poisson's ratio at the early stage. According to the prediction, the Poisson's ratio of concrete decreases with the increase in hydration period. This is understandable that the formation of denser microstructure during the hydration replaces the solids in the place of water. Particularly, the greatest decrease in Poisson's ratio occurs until 10 days, and after 10 days, the decrease becomes very mild. A similar behaviour was also observed by Narayan Swamy [58]. Therefore, to understand and

overcome the discrepancy in early-stage prediction, more validations with independent sets of experiments are required and left for the future work.

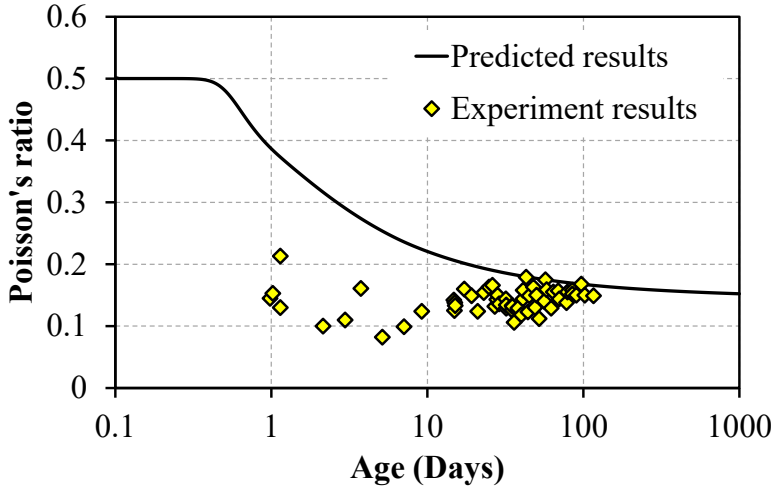

Figure. 15. Validation of Poisson's ratio of concrete with hydration period (the experimental data were obtained from ref. [63])

3.6 Effect of ITZ on Young's modulus and Poisson's ratio of mortar and concrete.

The Young's moduli of mortar and concrete computed with and without considering the ITZ are compared in **Figure. 16** for different w/c ratios. The considered fine aggregate volume fraction for mortar is 0.6 and cement: fine aggregate: coarse aggregate weight ratio for concrete is 1: 1.5: 3.2. It is evident that the model overestimates the modulus when the effect of ITZ is neglected for both mortar and concrete (**Figure. 16(a)** and **Figure. 16(b)**, respectively). Besides, the variation of Young's modulus between the cases of with and without ITZ decreases with increasing hydration period. As mentioned earlier, ITZ can also be considered as a distinct cement paste with low amount of clinker and high amount of water [6,35,64,65]. At the early age, the ITZ remains the weakest region with very high amount of porosity. However, during the hydration process, the ITZ becomes hardened cement paste with increased mechanical properties. Owing to the above reason, the variation in later age appeared to be decreasing. Relatively a similar tendency can be observed for all the w/c ratios

(**Figure. 16**). However, the deviation observed for concrete (**Figure. 16(b)**) is higher compared to the mortar results (**Figure. 16(a)**), which is mainly due to the higher ITZ effect in concrete (attributing to fine aggregate and coarse aggregate). For instance, after one day of w/c for 0.4 mortar, the modulus of without-ITZ case is approximately 40 % higher than that of with-ITZ case, whereas the variation after 28 days is reduced to around 10 % (see **Figure. 16(a)**). For the w/c 0.4 of concrete, after one day, the modulus of without-ITZ case is approximately 60 % higher than that of with-ITZ case, while the variation after 28 days is reduced to around 20 % (in **Figure. 16(b)**).

The difference between with ITZ and without ITZ cases is observed to increase with w/c ratio for both the mortar and concrete. This could be due to the high migration of free water to the surface of aggregates for high w/c matrix. In fact, the rate of migration is higher for the paste with higher w/c ratios; as the result, there would be a higher w/c ratio in ITZ, while the remaining paste would have a lower ratio. Since the elastic properties of the matrix and the ITZ are directly related to the water content and their porous structure, greater migration process of the water (at higher w/c ratio) led to more negative effect on Young's modulus. Similar observation was reported by Simeonov and Ahmad [26].

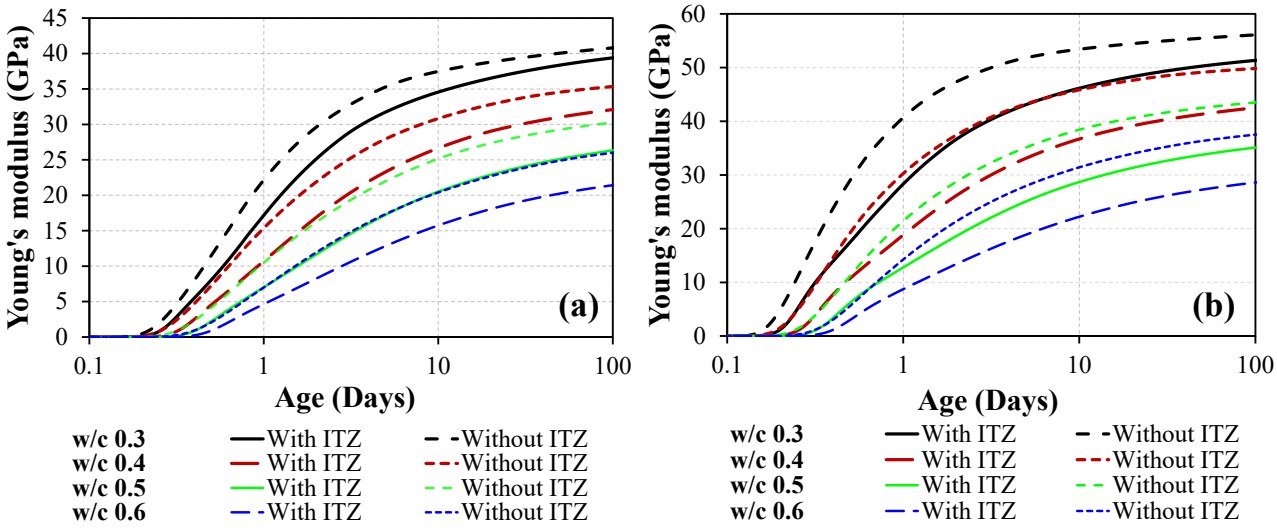

Figure. 16. Comparison of predicted Young's modulus of **(a)** mortar and **(b)** concrete for the cases of with and without ITZ for w/c 0.3-0.6

551

552 The comparison of predicted Poisson's ratio of mortar and concrete for the cases with and without
553 ITZ is depicted in **Figure. 17**. The results presented herein are corresponding to the w/c ratio of 0.3-
554 0.6 and to the fine aggregate volume fraction of 0.6 for mortar whereas cement: fine aggregate: coarse
555 aggregate weight ratio for concrete is 1: 1.5: 3.2. It can be seen that in the predicted results of both
556 cases, the Poisson's ratio increases with increase in w/c ratio, which is in consistent with the tendency
557 reported by Stefan et al. [55]. If the mortar and concrete is considered as two-phase matrix by
558 neglecting ITZ, the effective Poisson's ratio is stiffer than that predicted for with-ITZ case for all w/c
559 ratios as reflected in **Figure. 17**. Moreover, the variation between the predicted results from both
560 cases reduce with hydration period, which is probably because the mortar and concrete matrix become
561 hardened solid including ITZ due to the hydration process of clinker. Nevertheless, the deviation
562 observed for concrete (**Figure. 17(b)**) is higher compared to the mortar results (**Figure. 17(a)**), which
563 is mainly due to the higher ITZ effect in concrete (attributing to fine aggregate and coarse aggregate).
564 For instance, after one day of w/c for 0.4 mortar, the Poisson's ratio of without-ITZ case is
565 approximately 10 % lower than that of with-ITZ case, whereas the variation after 28 days is reduced
566 to around 2 % (see **Figure. 17(a)**). For the w/c 0.4 of concrete, after one day, the Poisson's ratio of
567 without-ITZ case is approximately 20 % lower than that of with-ITZ case, while the variation after
568 28 days is reduced to around 15 % (in **Figure. 17(b)**). Moreover, similar to that observed in Young's
569 modulus (refer to **Figure. 16**), the variation between with and without ITZ cases increase with w/c
570 ratio for both mortar and concrete.
571

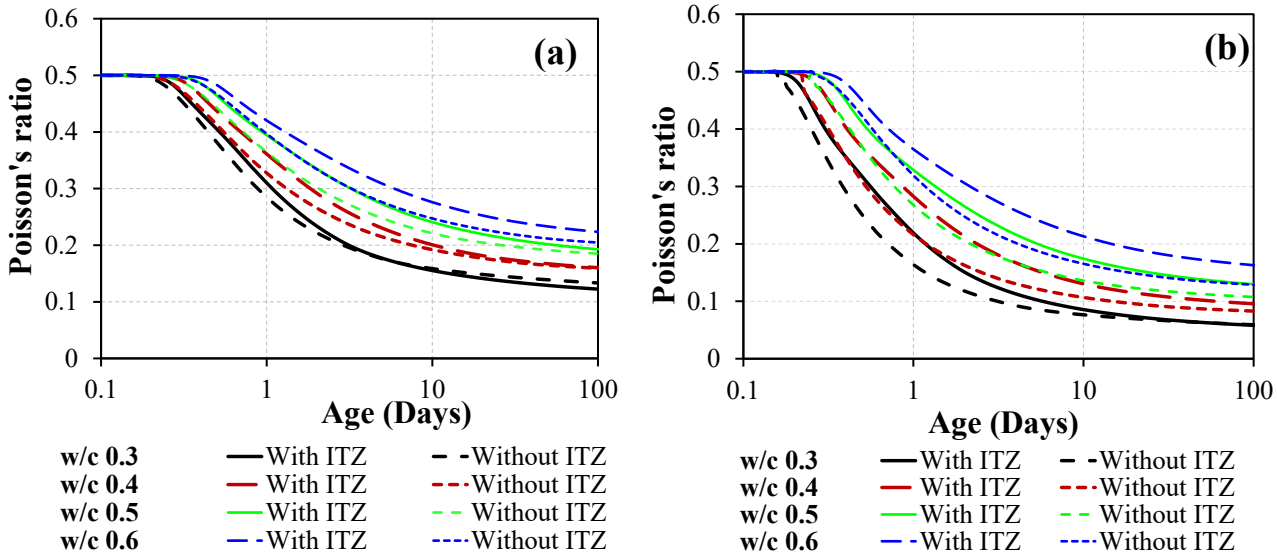

573 **Figure. 17.** Comparison of predicted Poisson's ratio of (a) mortar and (b) concrete for the cases of
574 with and without ITZ for w/c 0.3-0.6

575

576 **4. Conclusions**

577 In this research work, the mechanical properties such as Young's modulus and Poisson's ratio of
578 mortar and concrete were reliably predicted using the developed multi-scale model and
579 homogenization method. The mortars and concretes were assumed as three-phase composites, and
580 the ITZ for both coarse and fine aggregate were reliably considered as cement paste with high water
581 content. The mechanical properties of ITZ and bulk paste were based on the detailed microstructure
582 of hydrates during hydration reaction. The proposed models for mortar and concrete were validated
583 with experiment results for wide range of aggregate contents and w/c ratios.

584

585 The predicted Young's modulus excellently captured the realistic behaviour for the w/c ratios ranging
586 from 0.3 to 0.6 and aggregate content from 0.2 to 0.6. The computation of Poisson's ratio showed
587 relatively good agreement with the experimental data for mortar and concrete. However, the model
588 slightly overpredicted the Poisson's ratio at early stage (before 10 days) for concrete; thus, further
589 validations are recommended with more independent experimental results to generalize the Poisson's
590 ratio model of concrete. Moreover, the effect of ITZ on Young's modulus and Poisson's ratio were

591 demonstrated using the proposed model for mortar and concrete. At the same time, the results
592 predicted via typical way, i.e., two-phase model, was shown to reveal a stiffer material compared to
593 that of both experiment results and three-phase model for both mortar and concrete. The effect of ITZ
594 was higher for concrete compared to mortar due to the high amount of aggregates content.
595
596 Overall, the proposed novel three-phase models for mortar and concrete can be used to accurately
597 predict the mechanical properties. One of the marked merits of this model is, if the chemical
598 composition is known, the Young's modulus and Poisson's ratio can be computed, which would
599 reduce the waste of time, cost, material and manpower compared to typical approaches.
600
601 **Declaration of Competing Interest**
602 The authors declare that they have no known competing financial interests or personal relationships
603 that could have appeared to influence that work reported in this paper.
604
605 **References**
606
607 [1] J.C. Nadeau, A multiscale model for effective moduli of concrete incorporating ITZ water–
608 cement ratio gradients, aggregate size distributions, and entrapped voids, Cem. Concr. Res. 33
609 (2003) 103–113.
610 [2] M. Königsberger, M. Hlobil, B. Delsaute, S. Staquet, C. Hellmich, B. Pichler, Hydrate failure
611 in ITZ governs concrete strength: A micro-to-macro validated engineering mechanics model,
612 Cem. Concr. Res. 103 (2018) 77–94.
613 [3] Y. Elakneswaran, E. Owaki, S. Miyahara, M. Ogino, T. Maruya, T. Nawa, Hydration study of
614 slag-blended cement based on thermodynamic considerations, Constr. Build. Mater. 124
615 (2016) 615–625.
616 [4] N. Noguchi, S. Krishnya, T. Chabayashi, H. Kato, T. Nawa, Y. Elakneswaran, Hydration of
617 ferrite-rich Portland cement: Evaluation of Fe-hydrates and Fe uptake in calcium-silicate-

618 hydrates, Constr. Build. Mater. 288 (2021) 123142.
619 [5] Z. Hashin, P.J.M. Monteiro, An inverse method to determine the elastic properties of the
620 interphase between the aggregate and the cement paste, Cem. Concr. Res. 32 (2002) 1291–
621 1300.
622 [6] J.C. Nadeau, Water-cement ratio gradients in mortars and corresponding effective elastic
623 properties, Cem. Concr. Res. 32 (2002) 481–490.
624 [7] Y. Gao, C. Hu, Y. Zhang, Z. Li, J. Pan, Characterisation of the interfacial transition zone in
625 mortars by nanoindentation and scanning electron microscope, Mag. Concr. Res. 70 (2018).
626 [8] F. Bernard, S. Kamali-Bernard, Numerical study of ITZ contribution on mechanical behavior
627 and diffusivity of mortars, Comput. Mater. Sci. 102 (2015) 250–257.
628 [9] X. Zhu, Y. Yuan, L. Li, Y. Du, F. Li, Identification of interfacial transition zone in asphalt
629 concrete based on nano-scale metrology techniques, Mater. Des. 129 (2017) 91–102.
630 [10] Y. Gao, G. De Schutter, G. Ye, Z. Tan, K. Wu, The ITZ microstructure, thickness and porosity
631 in blended cementitious composite: Effects of curing age, water to binder ratio and aggregate
632 content, Compos. Part B Eng. 60 (2014) 1–13.
633 [11] A. Elsharief, M.D. Cohen, J. Olek, Influence of aggregate size, water cement ratio and age on
634 the microstructure of the interfacial transition zone, Cem. Concr. Res. 33 (2003) 1837–1849.
635 [12] Z. Zhu, J.L. Provis, H. Chen, Quantification of the influences of aggregate shape and sampling
636 method on the overestimation of ITZ thickness in cementitious materials, Powder Technol.
637 326 (2018) 168–180.
638 [13] H. Huang, Y. Yuan, W. Zhang, B. Liu, A. Viani, P. Mácová, Microstructure investigation of
639 the interface between lightweight concrete and normal-weight concrete, Mater. Today
640 Commun. 21 (2019) 100640.
641 [14] E. Khoury, B. Cazacliu, S. Remond, Control of effective water in recycled aggregate concrete
642 using power curves of the mixer, Mater. Today Commun. 21 (2019) 100721.
643 [15] Y. Jiang, T.C. Ling, M. Shi, Strength enhancement of artificial aggregate prepared with waste

644 concrete powder and its impact on concrete properties, J. Clean. Prod. 257 (2020) 120515.
645 [16] A. Ferraro, F. Colangelo, I. Farina, M. Race, R. Cioffi, C. Cheeseman, M. Fabbricino, Cold-
646 bonding process for treatment and reuse of waste materials: Technical designs and applications
647 of pelletized products, Crit. Rev. Environ. Sci. Technol. (2020) 1–35.
648 [17] M. Gesoğlu, T. Özturan, E. Güneyisi, Effects of cold-bonded fly ash aggregate properties on
649 the shrinkage cracking of lightweight concretes, Cem. Concr. Compos. 28 (2006) 598–605.
650 [18] P.J. Gunning, C.D. Hills, P.J. Carey, Production of lightweight aggregate from industrial waste
651 and carbon dioxide, Waste Manag. 29 (2009) 2722–2728.
652 [19] F. Colangelo, F. Messina, R. Cioffi, Recycling of MSWI fly ash by means of cementitious
653 double step cold bonding pelletization: Technological assessment for the production of
654 lightweight artificial aggregates, J. Hazard. Mater. 299 (2015) 181–191.
655 [20] Q. Chen, H. Zhu, Z. Yan, J.W. Ju, Z. Jiang, Y. Wang, A multiphase micromechanical model
656 for hybrid fiber reinforced concrete considering the aggregate and ITZ effects, Constr. Build.
657 Mater. 114 (2016) 839–850.
658 [21] B.F. Haile, D.W. Jin, B. Yang, S. Park, H.K. Lee, Multi-level homogenization for the
659 prediction of the mechanical properties of ultra-high-performance concrete, Constr. Build.
660 Mater. 229 (2019) 116797.
661 [22] Y. Li, Y. Li, Evaluation of elastic properties of fiber reinforced concrete with homogenization
662 theory and finite element simulation, Constr. Build. Mater. 200 (2019) 301–309.
663 [23] E. Gal, R. Kryvoruk, Meso-scale analysis of FRC using a two-step homogenization approach,
664 in: Comput. Struct., Pergamon, 2011: pp. 921–929.
665 [24] L. Brown, P.G. Allison, F. Sanchez, Use of nanoindentation phase characterization and
666 homogenization to estimate the elastic modulus of heterogeneously decalcified cement pastes,
667 Mater. Des. 142 (2018) 308–318.
668 [25] U.A. Nilsen, P.J.M. Monteiro, Concrete: A three phase material, Cem. Concr. Res. 23 (1993)
669 147–151.

[26] P. Simeonov, S. Ahmad, Effect of transition zone on the elastic behavior of cement-based composites, Cem. Concr. Res. 25 (1995) 165–176.

[27] M.P. Lutz, P.J.M. Monteiro, R.W. Zimmerman, Inhomogeneous interfacial transition zone model for the bulk modulus of mortar, Cem. Concr. Res. 27 (1997) 1113–1122.

[28] G. Li, Y. Zhao, S.S. Pang, Y. Li, Effective Young's modulus estimation of concrete, Cem. Concr. Res. 29 (1999) 1455–1462.

[29] F. Duplan, A. Abou-Chakra, A. Turatsinze, G. Escadeillas, S. Brule, F. Masse, Prediction of modulus of elasticity based on micromechanics theory and application to low-strength mortars, Constr. Build. Mater. 50 (2014) 437–447.

[30] F. Aouissi, C.C. Yang, A. Brahma, M. Bederina, Study of the influence of the interfacial transition zone on the elastic modulus of concrete using a triphasic model, J. Adhes. Sci. Technol. 30 (2016) 994–1005.

[31] S. Das, A. Maroli, N. Neithalath, Finite element-based micromechanical modeling of the influence of phase properties on the elastic response of cementitious mortars, Constr. Build. Mater. 127 (2016) 153–166.

[32] G. Ramesh, E.D. Sotelino, W.F. Chen, Effect of transition zone on elastic moduli of concrete materials, Cem. Concr. Res. 26 (1996) 611–622.

[33] S. Krishnya, Y. Yoda, Y. Elakneswaran, A two-stage model for the prediction of mechanical properties of cement paste, Cem. Concr. Compos. 115 (2021)

[34] J. Zheng, H.S. Wong, N.R. Buenfeld, Assessing the influence of ITZ on the steady-state chloride diffusivity of concrete using a numerical model, Cem. Concr. Res. 39 (2009) 805–813.

[35] J. Zheng, X. Zhou, X. Jin, An n-layered spherical inclusion model for predicting the elastic moduli of concrete with inhomogeneous ITZ, Cem. Concr. Compos. 34 (2012) 716–723.

[36] H. Ma, Z. Li, Multi-aggregate approach for modeling interfacial transition zone in concrete, ACI Mater. J. 111 (2014) 189–200.

696 [37] V. Maghsoodi, W/C Ratio Profile in ITZ of Mortar, Arab. J. Sci. Eng. 43 (2018) 1817–1824.
697 [38] Y. Li, Y. Li, R. Wang, Quantitative evaluation of elastic modulus of concrete with
698 nanoidentation and homogenization method, Constr. Build. Mater. 212 (2019) 295–303.
699 [39] E.J. Garboczi, D.P. Bentz, Analytical formulas for interfacial transition zone properties, Adv.
700 Cem. Based Mater. 6 (1997) 99–108.
701 [40] M. Rupasinghe, P. Mendis, T. Ngo, T.N. Nguyen, M. Sofi, Compressive strength prediction
702 of nano-silica incorporated cement systems based on a multiscale approach, Mater. Des. 115
703 (2017) 379–392.
704 [41] B. Lu, S. Torquato, Nearest-surface distribution functions for polydispersed particle systems,
705 Phys. Rev. A. 45 (1992) 5530–5544.
706 [42] E.J. Garboczi, D.P. Bentz, Multiscale Analytical/Numerical Theory of the Diffusivity of
707 Concrete, Adv. Cem. Based Mater. 8 (1998) 77–88.
708 [43] W. Dridi, Analysis of effective diffusivity of cement based materials by multi-scale modelling,
709 Mater. Struct. Constr. 46 (2013) 313–326.
710 [44] L.J. Parrot, D.C. Killoh, Prediction of Cement Hydration., in: Br. Ceram. Proc., 1984: pp. 41–
711 53.
712 [45] R.M. Christensen, K.N. Lo, Solutions for Effective Shear Properties in, J. Mech. Phys. Solids.
713 27 (1979) 315–330.
714 [46] T. Mori, K. Tanaka, Average stress in matrix and average elastic energy of materials with
715 misfitting inclusions, Acta Metall. 21 (1973) 571–574.
716 [47] G. Li, Y. Zhao, S.S. Pang, Four-phase sphere modeling of effective bulk modulus of concrete,
717 Cem. Concr. Res. 29 (1999) 839–845.
718 [48] X. Zhu, Y. Gao, Z. Dai, D.J. Corr, S.P. Shah, Effect of interfacial transition zone on the
719 Young's modulus of carbon nanofiber reinforced cement concrete, Cem. Concr. Res. 107
720 (2018) 49–63.
721 [49] E. Tsukahara, Y. Kato, T. Uomoto, Estimation Method of Young's Modulus of Mortar

722 Including Transition Zone at Aggregate Cement Paste Interface (in Japanese), Research
723 bulletin. 52 (2000) 333–336.
724 [50] H. Kawakami, The relationship between elastic modulus and age of mortar (In Japanese),
725 Concrete Engineering annual proceedings. 27 (2005).
726 [51] K.L. Scrivener, A.K.C. Lyon, F.P. Laugesen, The Interfacial Transition Zone (ITZ) Between
727 Cement Paste and Aggregate in Concrete, 2004.
728 [52] P. Wriggers, S.O. Moftah, Mesoscale models for concrete: Homogenisation and damage
729 behaviour, Finite Elem. Anal. Des. 42 (2006) 623–636.
730 [53] A. Teramoto, G. Igarashi, I. Maruyama, Study on the effect of aggrgate volume fraction on
731 dynamic elasticity in hardening process, Cem. Sci. Concr. Technol. (2011) 132–139.
732 [54] C. Di Bella, M. Wyrzykowski, M. Griffa, P. Termkhajornkit, G. Chanvillard, H. Stang, A.
733 Eberhardt, P. Lura, Application of microstructurally-designed mortars for studying early-age
734 properties: Microstructure and mechanical properties, Cem. Concr. Res. 78 (2015) 234–244.
735 [55] L. Stefan, F. Benboudjema, J.-M. Torrenti, B. Bissonnette, Prediction of elastic properties of
736 cement pastes at early ages, Comput. Mater. Sci. 47 (2010) 775–784.
737 [56] O. Bernard, F.-J. Ulm, E. Lemarchand, A multiscale micromechanics-hydration model for the
738 early-age elastic properties of cement-based materials, Cem. Concr. Res. 33 (2003) 1293–1309.
739 [57] I. Maruyama, G. Igarashi, Cement Reaction and Resultant Physical Properties of Cement Paste,
740 J. Adv. Concr. Technol. 12 (2014) 200–213.
741 [58] R. Narayan Swamy, Dynamic Poisson's ratio of portland cement paste, mortar and concrete,
742 Cem. Concr. Res. 1 (1971) 559–583.
743 [59] S.H. Han, J.K. Kim, Effect of temperature and age on the relationship between dynamic and
744 static elastic modulus of concrete, Cem. Concr. Res. 34 (2004) 1219–1227.
745 [60] V. Corinaldesi, G. Moriconi, Influence of mineral additions on the performance of 100%
746 recycled aggregate concrete, Constr. Build. Mater. 23 (2009) 2869–2876.
747 [61] H. Kawakami, A Study on the Relationship between Elastic Modulus and Compressive

748 Strength of Concrete (In Japanese), Concrete Engineering annual Proceedings. 28 (2006).
749 [62] N.S. Klein, L.A. Lenz, W. Mazer, Influence of the granular skeleton packing density on the
750 static elastic modulus of conventional concretes, Constr. Build. Mater. 242 (2020) 118086.
751 [63] A.E. Allos, L.H. Martin, Factors affecting Poisson's ratio for concrete, Build. Environ. 16
752 (1981) 1–9.
753 [64] A.K. Crumbie, Characerisation of the microstructure of concrete, PhD Diss. (1994).
754 [65] M. Sharma, S. Bishnoi, Influence of properties of interfacial transition zone on elastic modulus
755 of concrete: Evidence from micromechanical modelling, Constr. Build. Mater. 246 (2020)
756 118381.

757
758

759

760 **Appendix A: Material and experimental methodology**

761

762 Material

763 The cement used for experimental works of mortar was ordinary Portland cement (OPC). The
764 chemical composition and physical properties of the cement are detailed in **Table A1**. Fine aggregates
765 used were natural mountain sand with specific gravity of 2.57 g/cm^3, obtained from Kakegawa city
766 in Shizuoka prefecture of Japan.

767 **Table A1.** Chemical composition and physical properties of cement

Chemical composition (%)	SiO_2	20.89
	Al_2O_3	5.44
	Fe_2O_3	2.94
	Cao	65.11
	MgO	1.54
	SO_3	2.08
	Na_2O	0.27
	K_2O	0.53
	TiO_2	0.26

	P_2O_5	0.14
	MnO	0.05
	LOI	0.71
Physical properties	Blaine (cm^2/g)	3450
	Density (g/cm^3)	3.16

768

769 Mix design

770 The experiments were carried out for mortar at three different w/c: 0.3, 0.4 and 0.5 and two different
771 sand contents (in total volume fraction): 0.3 and 0.6. The mix proportions for each of these mixes are
772 stated in **Table A2.**

773

774 **Table A2.** Mixing proportion of mortar

Water (g)	Cement (g)	Sand (g)	w/c	Volume fraction of sand
1023	3408	2322	0.3	0.3
585	1947	4644		0.6
1173	2931	2322	0.4	0.3
669	1674	4644		0.6
1287	2571	2322	0.5	0.3
735	1470	4644		0.6

775

776 Sample preparation

777 According to mix proportion of mortar, φ50 x 100 mm cylinder samples were prepared. After
778 demolding, the samples were sealed and cured in an environment of 20 °C for 3, 7 and 28 days.

779 Young's modulus test

780 The Young's modulus was tested in accordance with JIS A 1149. The Young's modulus was the
781 average value of test results of three samples.

782 Poisson's ratio test

783 The Poisson's ratio experiment was carried out in accordance with JHS 307, and the Poisson's ratio
784 value was the average value of three samples.

785 Experiment results

786 The experiment results of Young's modulus and Poisson's ratio are shown in **Table A3** for three sets
787 of w/c and two sets of sand content.

788

789

790 **Table A3.** Mechanical properties of mortar

W/C	Sand (volume %)	Time (Days)	Young's modulus (kN/mm^2)	Poisson's ratio
0.3	30	3	-	0.218
		7	-	0.209
		28	-	0.203
	60	3	-	0.206
		7	-	0.183
		28	-	0.192
0.4	30	3	15.6	0.206
		7	18.7	0.197
		28	26.4	0.192
	60	3	20.0	0.216
		7	23.4	0.187
		28	25.5	0.186
0.5	30	3	9.56	0.179
		7	13.9	0.189
		28	16.6	0.212
	60	3	17.0	0.170
		7	21.1	0.176
		28	23.2	0.174

791